Journal of Energy Chemistry 32 (2019) 174–181

Contents lists available at ScienceDirect

Journal of Energy Chemistry

journal homepage: www.elsevier.com/locate/jechem

http://www.journals.elsevier.com/journal-of-energy-chemistry/

The template-assisted zinc ion incorporation in SAPO-34 and the enhanced ethylene selectivity in MTO reaction

Jiawei Zhong[a,b,e], Jingfeng Han[a], Yingxu Wei[a,*], Shutao Xu[a], Tantan Sun[a], Xinwen Guo[b], Chunshan Song[b,c], Zhongmin Liu[a,d,*]

[a] National Engineering Laboratory for Methanol to Olefins, State Energy Low Carbon Catalysis and Engineering R&D Center, Dalian National Laboratory for Clean Energy, iChEM (Collaborative Innovation Center of Chemistry for Energy Materials), Dalian Institute of Chemical Physics, Chinese Academy of Sciences, Dalian 116023, Liaoning, China

[b] State Key Laboratory of Fine Chemicals, PSU-DUT Joint Center for Energy Research, School of Chemical Engineering, Dalian University of Technology, Dalian 116024, Liaoning, China

[c] EMS Energy Institute, Departments of Energy and Mineral Engineering, and of Chemical Engineering, The Pennsylvania State University, University Park, PA 16802, USA

[d] State Key Laboratory of Catalysis, Dalian Institute of Chemical Physics, Chinese Academy of Sciences, Dalian 116023, Liaoning, China

[e] University of Chinese Academy of Sciences, Beijing 100049, China

ARTICLE INFO

Article history:
Received 4 July 2018
Revised 26 July 2018
Accepted 31 July 2018
Available online 10 August 2018

Keywords:
SAPO-34
Metal modification
MTO
Product selectivity
Ethylene

ABSTRACT

The SAPO-34 catalyst was fine-tuned with zinc cations through a straightforward template-assisted ion incorporation (TII) process, without the necessary template pre-removal and the preparation of NH_4-SAPO-34 intermediate, which is more facile, efficient and cost-effective than the conventional ion exchange process. The template-assisted zinc cations incorporated SAPO-34 catalysts were characterized by XRD, XRF, N_2 adsorption-desorption, XPS, SEM, EDX, ^{1}H NMR, respectively. Enhanced selectivity to ethylene and ratio of ethylene to propylene in MTO reaction are observed over the zinc cations modified SAPO-34 catalysts, due to the facilitated formation of lower methylbenzenes that favour the ethylene generation, as well as the increased diffusion hindrance originated from the zinc cations incorporation and the facilitated generation of aromatics compound.

1. Introduction

Light olefins including ethylene and propylene play vital roles in the petrochemical industry. The methanol-to-olefin (MTO) reaction, as a non-petrochemical route for the production of light olefins, with methanol produced from synthesis gas obtained by gasification of coal or biomass, has attracted great interests from both scientific and industrial field, due to the depletion of crude oil as well as the enormous world-wide market demand for light olefins [1]. Silicoaluminophosphate SAPO-34 is currently one of the most excellent industrial catalysts for the MTO reaction, owing to the small 8-ring pore openings (3.8 Å × 3.8 Å) and medium to strong acidity [2–4]. The hydrocarbon pool (HCP) mechanism has been proposed for MTO reaction, with the polymethylbenzenes and the corresponding carbenium ions as the important reaction intermediates, and the further evolution of HCP intermediate to bulky organic species as coke deposition results in the catalyst deactivation [5–7]. Marked dependence of product selectivity on the coke deposition has been observed over SAPO-34 catalyst, with the prolong of reaction time, and there are significant increases in ethylene selectivity and ratio ethylene to propylene with time, which is attributed to the enhanced diffusion restriction associated with the coke formation [7,8].

To date, a plethora of strategies (e.g. the incorporation of hierarchical structure [9–11], the optimization of acid property) have been developed to improve the catalytic performance of SAPO-34 catalyst in MTO reaction. In particular, the metal modification of SAPO-34 catalysts has attracted much attention in the past decades. For instance, the synthesis of MeASPO-34 with metal species isomorphously substituted into the framework of SAPO-34, a usually-adopted way to modify the cage structure, effectively optimises the acid property and adjusts the product selectivity [12–20]. By comparison, the ion-exchanged SAPO-34 has attracted

* Corresponding authors at: National Engineering Laboratory for Methanol to Olefins, State Energy Low Carbon Catalysis and Engineering R&D Center, Dalian National Laboratory for Clean Energy, iChEM (Collaborative Innovation Center of Chemistry for Energy Materials), Dalian Institute of Chemical Physics, Chinese Academy of Sciences, Dalian 116023, Liaoning, China.

E-mail addresses: liuzm@dicp.ac.cn (J. Zhong), weiyx@dicp.ac.cn (Y. Wei).

https://doi.org/10.1016/j.jechem.2018.07.017

little attention [21–24]. In general, enhanced selectivity to propylene is observed over SAPO-34 catalysts modified with metal modification, and the improved catalytic performance is usually ascribed to the optimization of acidity [6,25].

Recently, with the advantages of better metal dispersion, easy control of metal loading and simplicity in overall synthesis steps, the one-pot synthesis of Cu-SAPO-34 templated by Cu-amine (e.g. Tetraethylenepentamine (TEPA)) [26] complex or a combination of Cu-amine complex (e.g. Triethylenetetramine (TETA) [27], TEPA [28,29]) and traditional organic structure directing agents (OSDAs) has been developed, and applied in the selective catalytic reduction (SCR) of NO with NH_3. In addition to the one-pot synthesis of Me-SAPO-34, attentions are also paid to the direct template-assisted ion incorporation process without template pre-removal and the preparation of NH_4-SAPO-34 intermediate. For instance, our group found that the Cu-SAPO-34 prepared by the direct ion exchange process exhibits excellent catalytic performance in SCR reaction [30]. Our group also directly incorporated metal cations into the SAPO molecular sieve containing OSDA in a stainless steel vessel, but the samples experienced marked decrease in crystallinity under autogenous pressure [31]. Similarly, the Shenhua corporation in China patented the preparation method of Me-SAPO-34 from metal-complex by firstly mixing metal salt with OSDA during the synthesis procedure [32].

In our recent study, we demonstrated that the incorporated zinc cations via conventional ion exchange (CIE) process favour aromatic generation, the combined zinc cations accommodation and the facilitated aromatic formation introduce additional diffusion restriction for large-sized hydrocarbons, leading to increased selectivity to ethylene in MTO reaction [33]. Herein, SAPO-34 was modified with Zn cations through direct template-assisted ion incorporation (TII) process, without the tedious template pre-removal and the preparation of NH_4-SAPO-34 intermediate, which is much facile, cost-effective compared with the conventional ion exchange (CIE) process. Enhanced ethylene selectivity and ethylene-to-propylene ratio are observed over Zn-SAPO-34-TII catalysts, owing to the combination of the formation of specific HCP species as well as the enhanced diffusion hindrance. On one hand, the zinc cation incorporations facilitate the formation of lower methylbenzenes that favour ethylene production. On the other hand, the zinc cation incorporations facilitate the generation of aromatics, in particular, the bicyclic aromatics, rendering enhanced diffusion restriction.

2. Experimental

2.1. Synthesis of the materials

The zinc cations modified SAPO-34 was prepared by template-assisted ion incorporation (TII) process and conventional ion exchange (CIE) process, respectively.

For the TII process, the uncalcined SAPO-34 with the OSDA of triethylamine (TEA) (denoted as SP34) was stirred in 0.01 M $Zn(NO_3)_2{\cdot}6H_2O$ solution with liquid-to-solid (L/S) ratio of 30 mL/g at 50 °C for different hours (2 h, 4 h, 8 h), and then underwent filtration, washing and drying process. The sample stirred after 8 h was stirred in 0.01 M $Zn(NO_3)_2{\cdot}6H_2O$ solution with L/S ratio of 30 mL/g at 50 °C for another 8 h. The sample was calcined at 600 °C for 4 h, denoted as Zn-SP34-TII-2 h, Zn-SP34-TII-4 h, Zn-SP34-TII-8 h, Zn-SP34-TII-8h-T (T is short for Twice) [30].

For the CIE process, the uncalcined SAPO-34 with the OSDA of TEA (SP34) was calcined at 600 °C for 4 h to remove the OSDA. Then the calcined sample (denoted as H-SP34) was exchanged with 1 M NH_4NO_3 solution twice with L/S ratio of 10 mL/g at 80 °C for 2 h, and then underwent filtration, washing and drying process. The NH_4-SAPO-34 was exchanged with 0.01 M $Zn(NO_3)_2{\cdot}6H_2O$ solution with L/S ratio of 30 mL/g at 50 °C for 4 h, or for 8 h twice, and then underwent filtration, washing and drying process. The sample was calcined at 600 °C for 4 h. The obtained samples are denoted as Zn-SP34-CIE-4 h, Zn-SP34-CIE-8h-T.

2.2. Catalyst characterization

Powder X-ray diffraction (XRD) patterns were obtained on a PANalytical X'Pert PRO X-ray diffractometer at 40 kV and 40 mA with Cu K_α radiation ($\lambda = 1.54059$ Å).

The chemical composition was determined with a Philips Magix-601 X-ray fluorescence (XRF) spectrometer.

The nitrogen adsorption-desorption was performed on Micromeritics ASAP 2020 at − 196 °C. The sample was degassed at 350 °C under vacuum for 6 h before the measurements. The total surface area was calculated based on the BET equation. The micropore surface area and micropore volume were evaluated using the t-plot method. The total pore volume was calculated from nitrogen adsorbed volume at the relative pressure of 0.99.

X-ray photoelectron spectroscopy (XPS) was record with Thermo ESCALAB 250Xi with monochromatic Al K_α source (1486.6 eV, 15 kV, 10.8 mA). Binding energy (BE) values were referenced to the C 1*s* line at 284.8 eV.

Energy-dispersive X-ray spectroscopy (EDS) was conducted with cold field emission SEM Hitachi SU8020 equipped with a Horiba X-max silicon drift X-ray detector operated at an acceleration voltage of 20 kV.

The solid-state NMR spectroscopy was conducted with a Bruker Avance III 600 spectrometer equipped with a 14.1 T wide-bore magnet using a 4 mm H-X magic angle spinning (MAS) probe. For 1H MAS NMR spectra, the samples were dehydrated at 400 °C at a pressure of less than 10^{-3} Pa. The resonance frequencies were 600.13 MHz. Chemical shifts were referenced to admantane at 1.74 ppm.

2.3. MTO reaction test

The MTO reaction test was performed in a fixed bed reactor under atmospheric pressure. The catalyst (1000 mg, 40–60 mesh) was packed in the center of quartz wool. The sample was pretreated under a Ar flow at 550 °C for 45 min and then the temperature was adjusted to 475 °C. A methanol solution with a CH_3OH/H_2O weight ratio of 40/60 was pumped into the reactor with liquid pump (LC-05P), which gave the weight hourly space velocity (WHSV) of 2.0/h. The analysis of the composition of the exit gas was performed with an on-line gas chromatograph (Agilent GC 7890A) equipped with a flame ionization detector (FID) with capillary column CP-PoraPlot Q-HT (25 m × 0.32 mm × 20 μm) and thermal conductivity detector (TCD) with packed column Porapak QS (3 m × 2 mm). Hydrocarbons were analysed by FID, while CH_4, CO and CO_2 were analysed by TCD. CH_4 was taken as a reference bridge between FID signals and TCD signals. Conversions and selectivities were calculated on a carbon mole basis, selectivities are normalized by the total selectivity of the products observed, and dimethyl ether in the effluent is considered as a reactant.

2.4. Diffusion properties

The diffusion properties of probing molecule in the catalyst bed were evaluated with chromatographic method at 35 °C. The sample was heated from room temperature to 500 °C under a Ar flow for 1 h. Diffusion experiments were carried at 35 °C. Pulse containing ethylene (Ethylene 4.87%, He as the balance gas) was injected to catalyst bed for 0.6 s by switching a four-port valve, and the concentration of ethylene [$C(t)$] escaping from the catalyst bed was

detected by Pfeiffer Omnistar GSD 301 T3 Quadrapole Mass Spectrometer Gas Analyzer.

2.5. Analysis of retained organics

The amount of coke deposition in the catalysts after the MTO reaction was measured by thermogravimetry (TG) using a SDT Q600 analyzer. The catalysts were heated from room temperature to 900 °C under an air flow of 100 mL/min. The catalysts after methanol reaction at 475 °C for 2 min were kept isothermal in 150 °C for additional 30 min for complete removal of adsorbed water.

The retained organic species in the catalysts after the MTO reaction were post-treated with the dissolution/extraction procedure and analysed with GC–MS. The catalysts were dissolved in a HF solution (20 wt%), the organic compounds were extracted with a CH_2Cl_2 solution and analysed by an gas chromatograph (Agilent 7890A) equipped with an FID detector and a mass sensitive detector (Agilent 5795C) with a HP-5 capillary column (30 m, 0.25 mm i.d., stationary phase thickness 0.25 μm). The structures annotated onto the chromatograms are peak identifications reference to NIST database. The amount of hydrocarbon compounds was normalized with C_2Cl_6 as the internal standard.

3. Results and discussion

3.1. Comparison of TII and CIE process

As shown in Fig. S1, by contrast to H-SP-34 and Zn-SP34-CIE, the crystallinity of Zn-SP34-TII is maintained well, indicating the integrity of the texture property after the TII process. In addition, no diffraction peaks can be detected for ZnO crystallites (JCPD = 31.6°, 34.2°, 36.1°) [34], indicating that the exchanged metal species are dispersed homogeneously.

The bulk chemical compositions of as-prepared samples are analyzed with XRF. As shown in Table S1, zinc cations can be incorporated into the sample with OSDA of TEA via TII process, indicating that the small template molecules (e.g TEA) relative to the CHA cages are beneficial for the TII process, and no severe diffusion restriction during the incorporation of the metal cations into the crystals is observed, which is in consistence with our previous study [30]. In particular, under the identical exchange condition (exchange hours and times), Zn-SP34-TII exhibit much higher metal amount than Zn-SP34-CIE, indicating that the TEA template is beneficial for the direct zinc cations incorporation, which is also in good agreement to the report that the Cu-SP34 with TEA template shows higher copper amount than those with other investigated templates in the direct ion exchange process [30]. The sample Zn-SP34-TII is further investigated in the following part.

3.2. Influence factor of TII process

The influence of the ion exchange time and number of times are further studied. With the increase of exchange hour and the increased number of times (Twice), the incorporated zinc amount just increases slightly, from 0.74 wt% of Zn-SP34-TII-2 h to 0.79 wt% of Zn-SP34-TII-8h-T, indicating that satisfying zinc amount can be incorporated via TII process in quite short a time. Furthermore, no phases related to ZnO crystallites are observed over Zn-SP34-TII catalysts with the increase of exchange hour and the increased number of times, though the crystallinity of Zn-SP34-TII decreases slightly (Fig. S2).

The textual properties of the as-prepared samples are analyzed with nitrogen adsorption-desorption. As shown in Table 1, Zn-SP34-TII exhibits slight decrease in pore volume and surface area by contrast to H-SP34. In particular, with the same exchange time

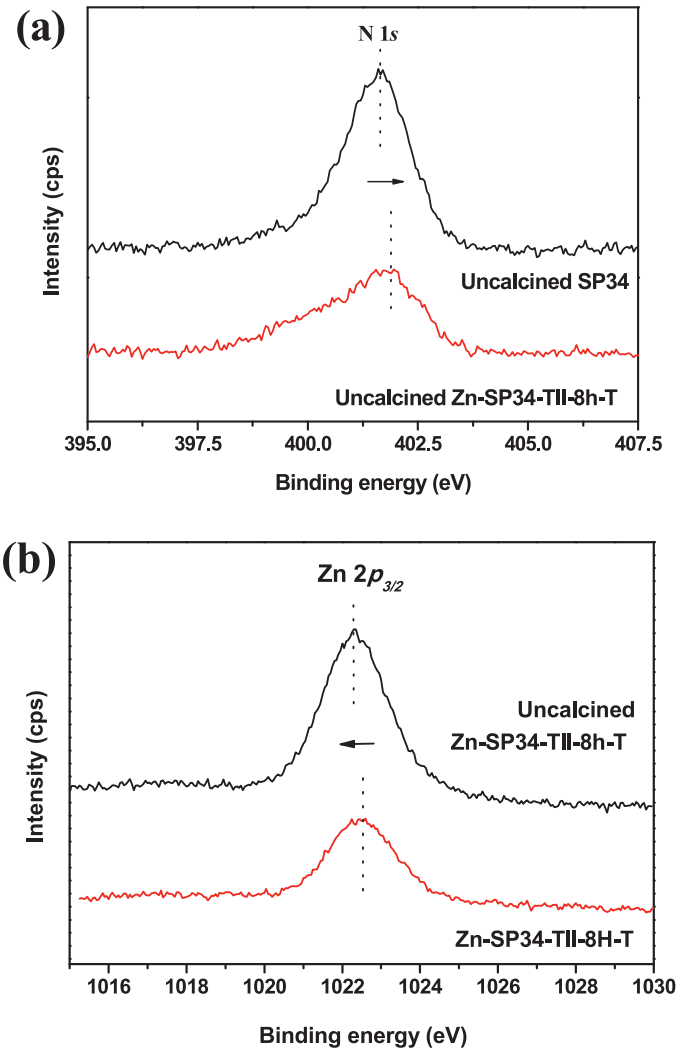

Fig 1. (a) N 1*s* XPS core level spectra for uncalcined SP34 and uncalcined Zn-SP34-TII-8h-T. (b) Zn $2p_{3/2}$ XPS core level spectra for uncalcined Zn-SP34-TII-8h-T and Zn-SP34-TII-8h-T after calcination.

(4 h), Zn-SP34-TII-4 h shows higher surface areas and pore volume than Zn-SP34-CIE-4 h, and even Zn-SP34-TII-8h-T with prolonged exchange time (8 h) and double exchange times (twice) exhibits higher surface areas and pore volume than Zn-SP34-CIE-4 h, indicating that the TII process effectively maintains the physical structure of the sample by contrast to the CIE process that requires the necessary template pre-removal and the preparation of NH_4-SAPO-34 intermediate.

3.3. The proposed mechanism of TII process

XPS is employed to investigate the electronic interaction between nitrogen atoms in the OSDA and Zn cations based on the binding energy (BE) shift of N 1*s* and Zn 2*p* (Fig. 1). The binding energy of N 1*s* spectra of uncalcined Zn-SP34-TII-8h-T is slightly higher than that of uncalcined SP34, indicating that the charge transfers from nitrogen atoms in TEA to Zn cations. Similarly, the binding energy of Zn $2p_{3/2}$ of the uncalcined Zn-SP34-8h-T is slightly lower than that of Zn-SP34-8h-T after calcination, which also confirms that the electron from nitrogen atoms in TEA transfers into the zinc cations, leading to increased electron density of zinc cations. Therefore, it is proposed that the nitrogen atoms in TEA function as the anchoring sites for the zinc cations during the TII process, which is in consistence with the various reported

Table 1. Textual properties of H-SP34, Zn-SP34-TII and Zn-SP34-CIE.

	Surface area (m^2/g)			Pore volume (cm^3/g)	
	S_{total}[a]	S_{micro}[b]	S_{ext}[c]	V_{total}	S_{total}[d]
H-SP34	506.42	479.79	26.62	0.27	0.23
Zn-SP34-TII-8h-T	458.46	440.82	17.63	0.27	0.22
Zn-SP34-TII-4h	473.86	452.27	21.58	0.27	0.22
Zn-SP34-CIE-4h	438.76	420.86	17.90	0.25	0.21

[a] BET surface area.
[b] t-plot micropore surface area.
[c] t-plot external surface area.
[d] t-plot micropore volume.

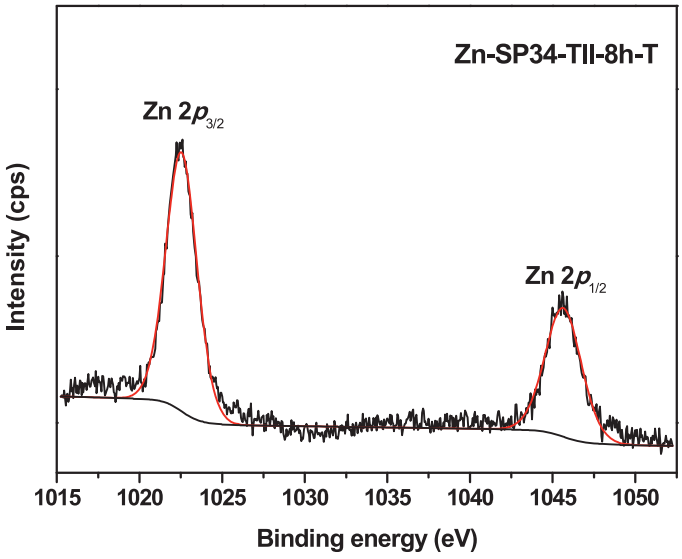

Fig 2. Zn 2*p* XPS core level spectra for Zn-SP34-TII-8h-T.

nitrogen doping strategies in the support modification and the consequent enhanced metal-support interaction via electron transfer [35–37].

In addition, based on the interaction of zinc cation and the nitrogen atoms of TEA template, the proposed coordination structure of the zinc species in the uncalcined Zn-SP34-8h-T is provided in Scheme S1. The Zn ions are coordinated with the nitrogen atom in TEA template in addition to three oxygen atoms in the CHA framework and two water molecules [30,38].

3.4. The chemical state and metal distribution

XPS is further employed to confirm the chemical state of Zn species in Zn-SP34-TII-8h-T (Fig. 2). Zn-SP34-TII-8h-T exhibits binding energy of Zn $2p_{1/2}$ core level at 1045.6 eV and Zn $2p_{3/2}$ core level at 1022.5 eV, and the area of Zn $2p_{1/2}$ peak is roughly half the area of Zn $2p_{3/2}$ peak. The Zn $2p_{1/2}$ peak and Zn $2p_{3/2}$ peak are narrow and symmetrical, indicating that zinc species exist in a single chemical state [34]. The zinc species localized at the cation exchanged sites generally exhibit a high BE than ZnO, owing to the higher electronegativity of the lattice oxygen of the molecular sieve than that of the O^{2-} ligand in ZnO [39–41]. Therefore, the peak with BE 1022.5 eV is assigned to isolated Zn^{2+} cations being stabilized at the exchangeable sites [42,43].

As shown in Table 2, for Zn-SP34-TII-8h-T, the Zn/Si molar ratio near the external surface (0.19) is higher than that in the bulk (0.11), and the calculated zinc content near the external surface is 2.89 wt%, which is also higher than that in the bulk (0.79 wt%); therefore, in the TII process, the zinc cations are mainly incorporated at the periphery of the crystals, which is attributed to the enrichment of Si atoms in the sublayer near the external surface of SAPO-34 [2,44,45].

Table 2. The composition and metal distribution in H-SP34 and Zn-SP34-TII-8h-T.

Elemental composition of H-SP34 (mol %)	Bulk[a]	$Si_{0.071}Al_{0.522}P_{0.407}$
	Surface[b]	$Si_{0.132}Al_{0.521}P_{0.347}$
	R_{Si}[c]	1.9
Zn/Si molar ratio in Zn-SP34-TII-8h-T	Bulk[a]	0.11
	Surface[b]	0.19
	R_{Zn}[c]	1.7

[a] Determined by XRF.
[b] Determined by XPS.
[c] Surface Si(Zn) enrichment index de-fined as $[Si/(Si+P+Al)]_{surface}/[Si/(Si+P+Al)]_{bulk}$ and $(Zn/Si)_{surface}/(Zn/Si)_{bulk}$.

The Si enrichment and the resulting Zn enrichment near the external surface were further confirmed by the EDX analysis (Fig. S3). Zn-SP34-TII-8h-T was ground severely so as to expose the inner part of crystals, and the EDX analysis of the ground sample is provided. As shown in the EDX analysis along the scan direction, the relative ratio of P to Al maintains constant basically, while the relative ratios of Zn to Al and Si to Al decrease gradually from the external surface to the inner part of the crystals, indicating that the Zn species and Si species are relatively enriched in the sublayer near the external surface, while the structural elements such as P and Al are basically homogeneously distributed throughout the crystals [33,46].

3.5. MTO reaction test

The influences of the ion exchange factors (exchange hour and number of times) of the TII process on the catalytic performance in MTO reaction were investigated. Methanol conversion over H-SP34 and Zn-SP34-TII with different exchange hour and number of times was performed at 475 °C with WHSV of 2 h^{-1}. As shown in Fig. 3, the incorporation of zinc cations increases the initial selectivity to ethylene, and there is a basically positive correlation between the increase in ethylene selectivity and the exchange hour and number of times. The highest selectivity to ethylene is achieved in Zn-SP34-TII-8h-T, implying that the increased exchange hours and doubled number of times is beneficial for the generation of ethylene, which might be related to the higher amount of zinc cations incorporated into the sublayer near the external surface, which will be discussed in the following parts [33].

The catalytic performance of methanol conversion over H-SP34 and Zn-SP34-TII-8h-T was further deeply discussed. As shown in Fig. 4, the Zn cations modification remarkably facilitates the production of ethylene, consequently increasing the selectivity to light olefins. After the identical reaction time of 2 min, enhanced ethylene selectivity of 35% and selectivity to light olefins of 75% are observed over Zn-SP34-TII-8h-T-2 min compared with H-SP34-2 min, and the selectivity of ethylene and light olefins over Zn-SP34-TII-8h-T-2 min is 5.5% and 7.5% higher than those over H-SP34-2 min. In addition, the highest selectivity (HS) of light olefins of about

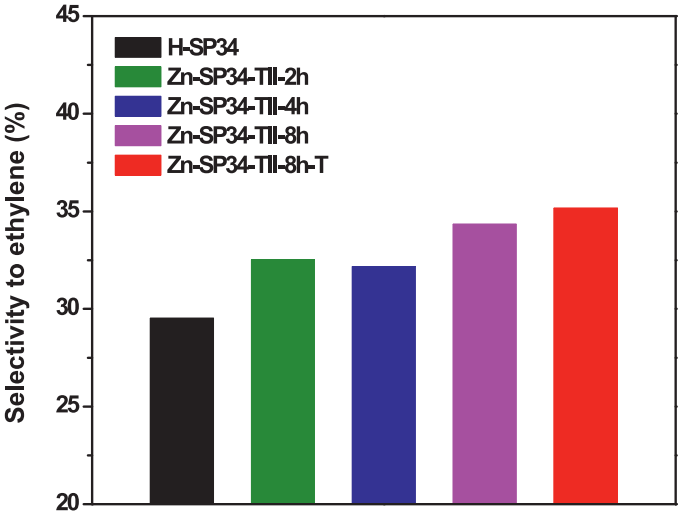

Fig 3. The selectivity to ethylene of MTO reaction over H-SP34 and Zn-SP34-TII with different exchange hours and number of times.

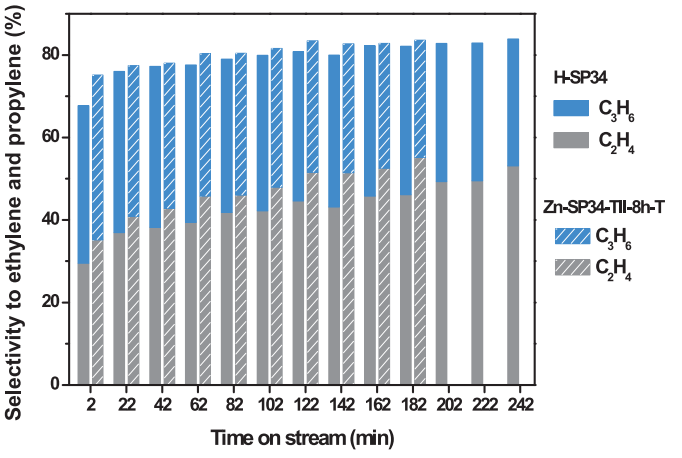

Fig 4. The selectivity to light olefins in MTO reaction over H-SP34 and Zn-SP34-TII-8h-T.

83%, nearly identical to H-SP34-HS, can be achieved over Zn-SP34-TII-8h-T-HS in a shorter reaction time (182 min) compared with H-SP34-HS (242 min). Therefore, the zinc cations modification not only markedly enhances the ethylene selectivity, but also efficiently achieves highest selectivity to light olefins with much shorter reaction time.

As shown in the products distribution and ratio of ethylene to propylene (Fig. 5), accompanied with the increased selectivity to ethylene, the selectivity to large-sized hydrocarbons such as propylene, C4, C5 and C6 decreases markedly, rendering remarkable increase in the ratio of ethylene to propylene, which is of great practical significance due to the relatively higher added value of ethylene than that of propylene. In addition, after zinc cation modification, only neglectable amount of CO (the selectivity of CO increases from 0.12% to 0.14%) and no CO_2 are detected by TCD, implying that no methanol decomposition is triggered by the zinc cations incorporation [33,47], which is different from the Cu-based catalysts active for methanol synthesis as well as methanol decomposition based on microscopic reversibility [48]. And the catalyst lifespan of Zn-SP34-TII-8h-T only slightly decreases (Fig. S4).

3.6. The acidity

In previous studies, the improved catalytic performance over SAPO-34 catalysts modified with metal species is usually ascribed to the optimization of acidity. As shown in the ^{1}H MAS NMR spectra (Fig. 6), signal at 3.6 ppm is characteristic of acidic bridging Si(OH)Al groups [49], the density of Si(OH)Al for H-SP34 and Zn-SP34-TII-8h-T is 0.51 and 0.40 mmol/g, respectively, indicating that protons from Brønsted acid sites are partly substituted by the incorporated zinc cations, which is in agreement with the XPS analysis that isolated Zn^{2+} species are stabilized at the exchangeable sites. In general, enhanced selectivity to propylene is achieved over SAPO-34 catalysts with lower acid density, owing to the retarded side reactions such as the hydrogen transfer reactions that consume generated olefins (e.g propylene) [6,25]. Therefore, the reason associated with the adjustment of acidity can be excluded, and factors other than the adjustment of acidity should account for the increased ethylene selectivity over zinc cations modified SAPO-34 catalysts observed in this study.

3.7. The diffusion property

In general, a heterogeneous gas-solid catalytic reaction involves the following steps, the adsorption of reactants in gas phase on solid surface, the surface reaction of adsorbed species, as well as desorption of generated products to the gas phase. Thus the intracrystalline mass transport of the generated products out of the CHA cavity in SAPO-34 catalysts plays a vital role in the MTO reaction. Chromatographic method is adopted to investigate the impacts originated from the zinc cation incorporation and coke deposition on the diffusion property of probing molecular (e.g ethylene) in the catalyst bed. The residence time distribution (RTD) of ethylene was calculated according to Eq. (1). Through the contrarian strategy of diffusion of probing molecular into the catalyst bed, the valuable mass transport properties of the main products (e.g ethylene) from the CHA cage to the gas phase can be obtained. The diffusion properties of ethylene in the catalyst bed of fresh catalysts (H-SP34 and Zn-SP34-TII-8h-T), catalysts after reaction for 2 min (H-SP34-2 min, Zn-SP34-TII-8h-T-2 min) as well as catalysts with the highest selectivity (HS) to light olefins (H-SP34-HS, Zn-SP34-TII-8h-T-HS) were evaluated, and the residence time distribution (RTD) was calculated by the following equation:

$$E(t) = \frac{C(t)}{\int_0^\infty C(t)\mathrm{d}t}$$

Where $C(t)$ is concentration of probe molecules exiting the catalyst bed, and t is time.

As shown in Fig. 7, over the as-prepared catalysts, H-SP34 and Zn-SP34-TII-8h-T, dispersive RTD profiles and relatively longer mean residence time are observed, implying that the intracrystal diffusion should be the main diffusion mode for probing molecular over the fresh catalyst. It should be noted that relatively shorter residence time is obtained over Zn-SP34-TII-8h-T than that over H-SP34, indicating that the zinc cations are successfully incorporated into the CHA cavity of SAPO-34 catalysts.

Furthermore, shorter residence time and sharper RTD profile are observed over Zn-SP34-TII-8h-T-2 min compared with H-SP34-2 min, indicating that the probing molecules encountered increased diffusion hindrance over Zn-SP34-TII-8h-T-2 min. Therefore, it is deduced that the generated products encounter markedly severer diffusion restriction during the diffusion path from CHA cages to the gas phase over Zn-SP34-TII-8h-T-2 min than H-SP34-2 min. It is widely accepted that the bulky hydrocarbons (e.g propylene, C4, C5 and C6) exhibit relatively lower diffusivity than the counterparts with small molecular size (e.g ethylene) [33]; therefore, the generated propylene and other bulky hydrocarbons encounter much

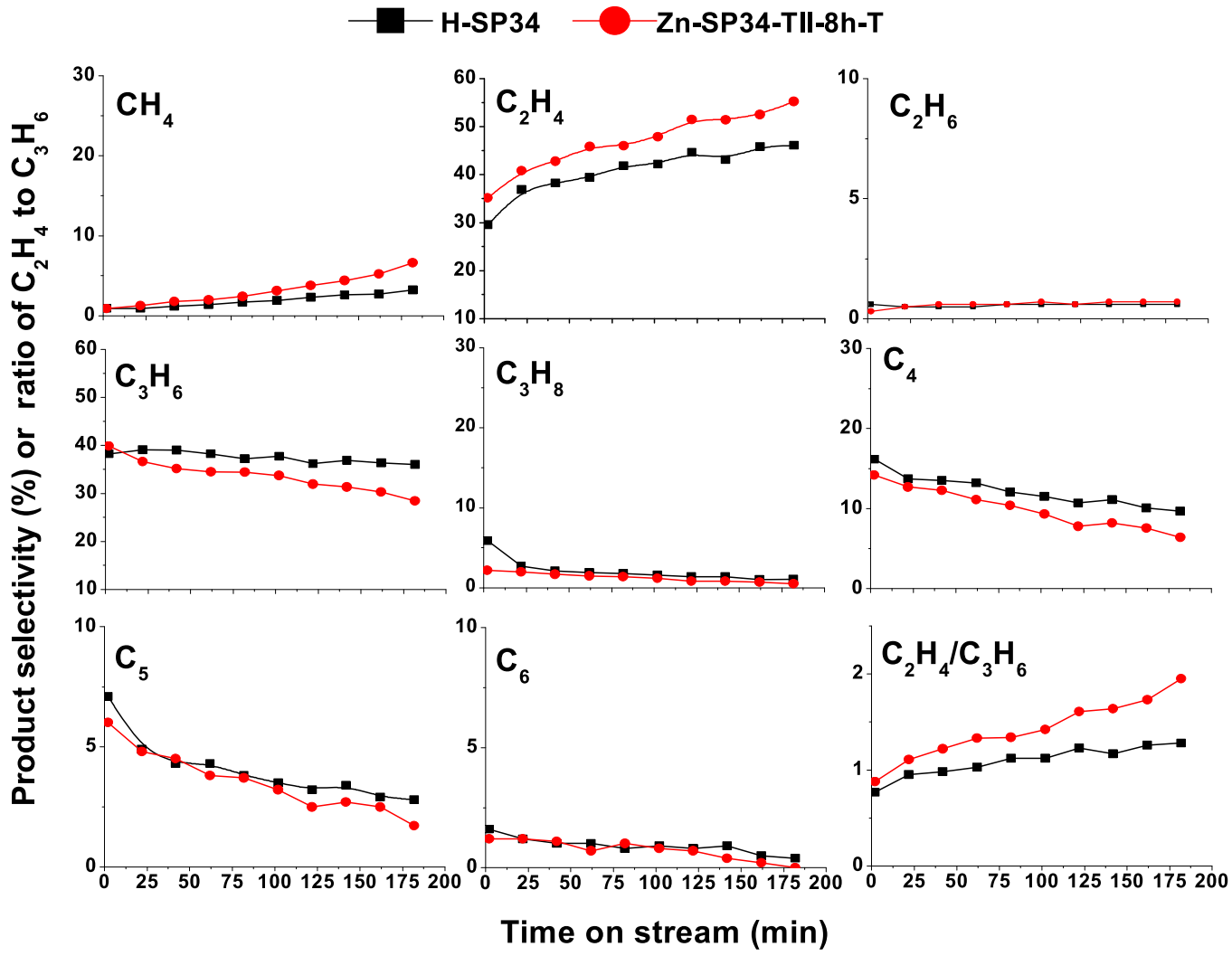

Fig 5. Products distribution and ratio of C_2H_4 to C_3H_6 of MTO reaction over H-SP34 and Zn-SP34-TII-8h-T.

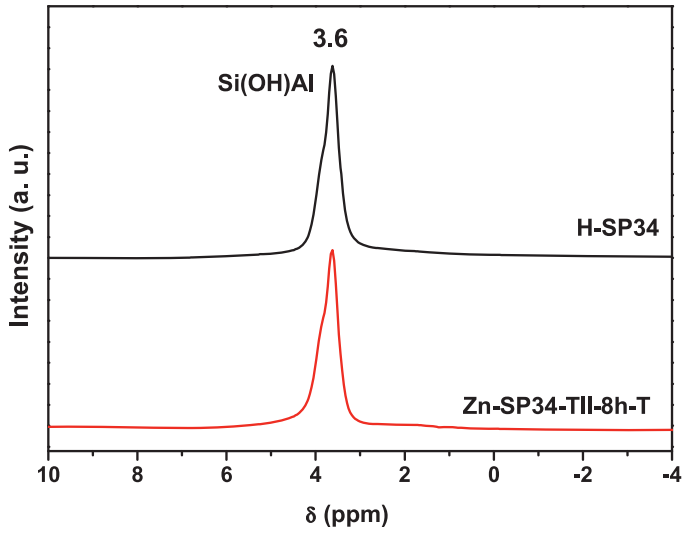

Fig 6. Solid-state 1H MAS NMR spectra of the H-SP34 and Zn-SP34-TII-8h-T.

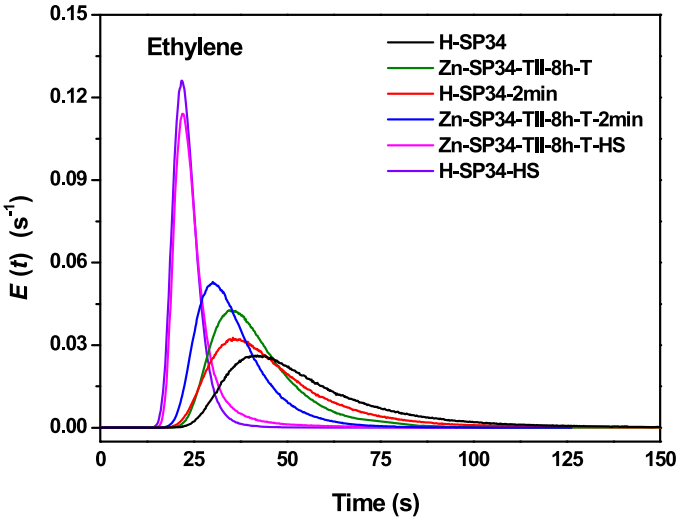

Fig 7. The influence of zinc cations incorporation and coke deposition on (RTD) of ethylene in the catalyst bed of different catalysts.

more marked diffusion hindrance than ethylene over Zn-SP34-TII-8h-T-2 min, which results in significantly higher selectivity of ethylene over Zn-SP34-TII-8h-T-2 min (Figs. 4 and 5).

Moreover, sharpest and most narrow RTD profiles are observed over the catalysts with highest selectivity to light olefins (H-SP34-

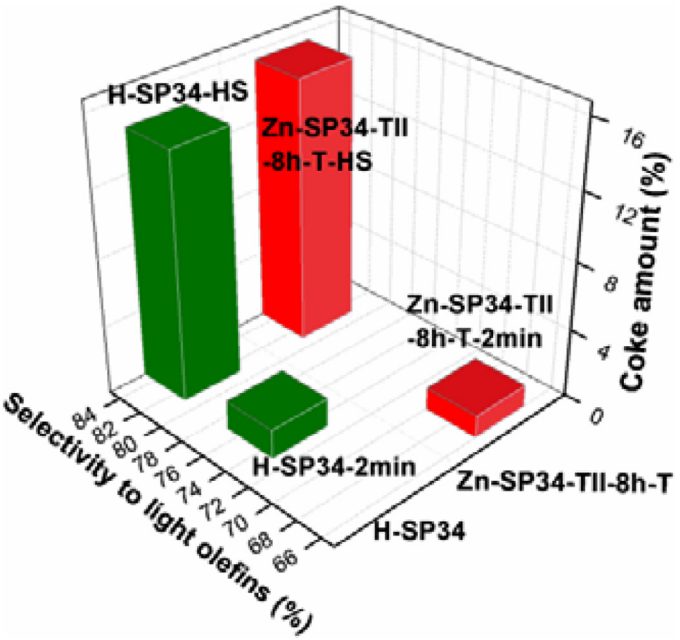

Fig 8. The relationship between coke amount and selectivity to light olefins over H-SP34 and Zn-SP34-TII-8h-T after different reaction times.

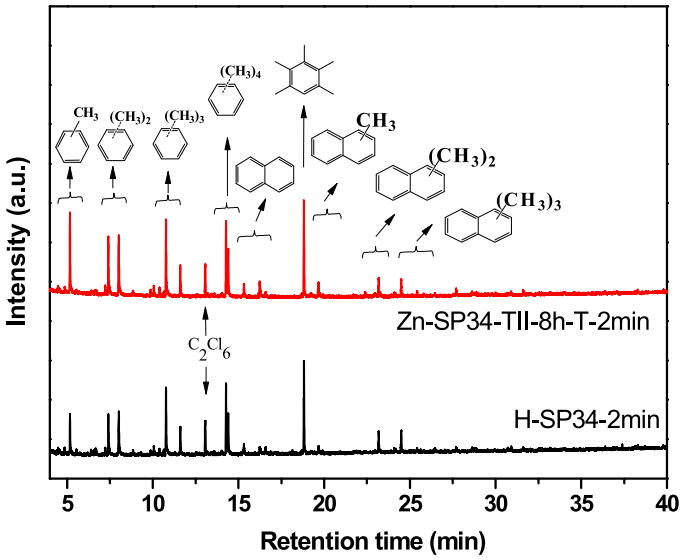

Fig 9. GC-MS chromatograms of coke species in H-SP34-2 min and Zn-SP34-TII-8h-T-2 min.

HS, Zn-SP34-TII-8h-T-HS), implying the direct penetration of the probing molecular in the catalyst bed via intercrystalline diffusion. And the relatively sharper RTD profile over H-SP34-HS compared with Zn-SP34-TII-8h-T-HS might be related with different coke amounts, which will be discussed in the following part.

3.8. Analysis of retained organics

As shown in the relationship between coke amount and selectivity to light olefins (Fig. 8), after the same reaction time (2 min), enhanced selectivity to light olefins of 75% is obtained over Zn-SP34-TII-8h-T-2 min with nearly identical coke amount (1.7 wt%) by contrast to H-SP34-2 min (1.3 wt%). The slightly increased coke amount over Zn-SP34-TII-8h-T-2 min compared with H-SP34-2 min indicates that the zinc cations incorporation exert some kind of effect similar to pre-coking process, which is in good agreement with the enhance diffusion restriction of probing molecule encountered over Zn-SP34-TII-8h-T-2 min (Fig. 7). Moreover, the highest selectivity (HS) to light olefin of approximately 83% is achieved over Zn-SP34-TII-8h-T-HS with lower coke deposition (14.5 wt%), compared with the H-SP34-HS (15.5 wt%), which is also in consistence with the severer diffusion limitation over H-SP34-HS than Zn-SP34-TII-8h-T-HS (Fig. 7). Therefore, the zinc cations modification not only significantly enhance the initial selectivity to ethylene and ratio of ethylene to propylene, but also achieve the highest selectivity to light olefins with much shorter reaction time at the expense of lower coke deposition.

The deposited coke species in samples after reaction of 2 min were extracted and analyzed by GC-MS (Fig. 9). The aromatic compounds including methyl-substituted benzenes, naphthalenes and methyl-substituted naphthalenes appear among the confined organic species in H-SP34-2 min and Zn-SP34-TII-8h-T-2 min. However, it should be noted that lower methylbenzenes with one to three methyl group become predominant in Zn-SP34-TII-8h-T-2 min, which is in consistence with the report that HCP species containing benzene molecules with four or more methyl groups facilitate propene production, while those with two or three methyl groups favor ethylene generation [50,51]. Furthermore, slight increased amount of naphthalene and methyl-substituted naphthalenes is observed over Zn-SP34-TII-8h-T-2 min, which might be attributed to the facilitated aromatics generation by zinc cations via dehydrogenation [40], or the hydrogen-transfer reaction between the methylbenzene and methanol via the synergism between Brønsted acid sites and Lewis acid sites [52]. Combined with the result mentioned above that the zinc cations are mainly located in the CHA cavity near the external surface, it is reduced that the formation of bicyclic species is also mainly located in the sublayer at the periphery of the crystals. Therefore, it is proposed that the zinc cations incorporation not only facilitates the generation of HCP species such as lower methylbenzenes that favour the ethylene production, but also promotes the formation of naphthalene and methyl-substituted naphthalenes in the sublayer near external surface that leads to the enhanced diffusion hindrance for the products especially the bulky hydrocarbon (e.g. propylene).

4. Conclusions

The SAPO-34 was modified with zinc cations through a straightforward template-assisted ion incorporation (TII) process, without template pre-removal and the preparation of NH_4-SAPO-34 intermediate, which is much more facile and cost-effective than the tedious conventional ion exchange process. On one hand, the zinc cation incorporation facilitates the formation of HCP species such as lower methylbenzenes that favour ethylene generation. On the other hand, the zinc cation incorporation and the facilitated formation of aromatics especially bicyclic species (e.g. naphthalene and methyl-substituted naphthalenes) in the CHA cavities of sublayer near the external surface increase the diffusion hindrance for the olefins products especially the large-sized hydrocarbon (e.g. propylene). The combined effects result in the remarkably enhanced selectivity to ethylene in MTO reaction.

Conflict of interest

The authors declare that they have no conflict of interest.

Acknowledgments

We are grateful to the National Natural Science Foundation of China (21603223, 91745109, 91545104, 21473182, 91334205)

and the Youth Innovation Promotion Association of the Chinese Academy of Sciences (2014165) for financial support.

Supplementary materials

Supplementary material associated with this article can be found, in the online version, at doi:10.1016/j.jechem.2018.07.017.

References

[1] S. Kvisle, T. Fuglerud, S. Kolboe, U. Olsbye, K.P. Lillerud, B.V. Vora, Methanol–to-hydrocarbons, in: G. Ertl, H. Knözinger, F. Schüth, J. Weitkamp (Eds.), Handbook of Heterogeneous Catalysis, Wiley-VCH Verlag GmbH& Co. KGaA, Weinheim, 2008, pp. 2950–2965.
[2] P. Tian, Y. Wei, M. Ye, Z. Liu, ACS Catal 25 (2015) 1922–1938.
[3] J. Zhong, J. Han, Y. Wei, P. Tian, X. Guo, C. Song, Z. Liu, Catal. Sci. Tech 7 (2017) 4905–4923.
[4] Q. Sun, Z. Xie, J. Yu, Natl. Sci. Rev 0 (2017) 1–17.
[5] U. Olsbye, S. Svelle, K.P. Lillerud, Z. Wei, Y. Chen, J. Li, J. Wang, W. Fan, Chem. Soc. Rev 44 (2015) 7155–7176.
[6] S. Xu, Y. Zhi, J. Han, W. Zhang, X. Wu, T. Sun, Y. Wei, Z. Liu, Advances in catalysis for methanol-to-olefins conversion, in: C. Song (Ed.), Advances in Catalysis, 61, Academic Press, 2017, pp. 37–122.
[7] U. Olsbye, S. Svelle, M. Bjorgen, P. Beato, T.V. Janssens, F. Joensen, S. Bordiga, K.P. Lillerud, Angew. Chem. Int. Ed 51 (2012) 5810–5831.
[8] B.P.C. Hereijgers, F. Bleken, M.H. Nilsen, S. Svelle, K.P. Lillerud, M. Bjorgen, B.M. Weckhuysen, U. Olsbye, J. Catal 264 (2009) 77–87.
[9] Y. Wei, T.E. Parmentier, K.P. de Jong, J. Zečevi, Chem. Soc. Rev 44 (2015) 7234–7261.
[10] J. Perez-Ramirez, C.H. Christensen, K. Egeblad, C.H. Christensen, J.C. Groen, Chem. Soc. Rev 37 (2008) 2530–2542.
[11] D.P. Serrano, J.M. Escola, P. Pizarro, Chem. Soc. Rev 42 (2013) 4004–4035.
[12] A.Z. Varzaneh, J. Towfighi, S. Sahebdelfar, Micro. Meso. Mater 236 (2016) 1–12.
[13] A. Amoozegar, M. Haghighi, S. Aghamohammadi, RSC Adv 6 (2016) 51024–51036.
[14] E. Aghaei, M. Haghighi, Z. Pazhohniya, S. Aghamohammadi, Micro. Meso. Mater 226 (2016) 331–343.
[15] T. Inui, M. Kang, Appl. Catal. A Gen 164 (1997) 211–223.
[16] M. Kang, J. Mol. Catal. A Chem. 150 (1999) 205–212.
[17] M. Kang, C.T. Lee, M.H. Um, J. Ind. Eng. Chem 5 (1999) 10–15.
[18] M. Kang, J. Mol. Catal. A Chem 160 (2000) 437–444.
[19] M. Salmasi, S. Fatemi, A.T. Najafabadi, J. Ind. Eng. Chem 17 (2011) 755–761.
[20] L. Xu, Z. Liu, A. Du, Y. Wei, Z. Sun, Stud. Surf. Sci. Catal 147 (2004) 445–450.
[21] M.A. Djieugoue, A.M. Prakash, L. Kevan, J. Phy, Chem. B 104 (2000) 6452–6461.
[22] Z. Zhu, M. Hartmann, L. Kevan, Chem. Mater 12 (2000) 2781–2787.
[23] S.J. Kim, J.W. Park, K.Y. Lee, G. Seo, M.K. Song, S.Y. Jeong, J. Nanosci. Nanotech 10 (2010) 147–157.
[24] H. Chae, S. Park, Y.H. Shin, M.B. Park, Micro. Meso. Mater 259 (2018) 60–66.
[25] D. Chen, K. Moljord, A. Holmen, Micro. Meso. Mater 164 (2012) 239–250.
[26] A. Turrina, E.C.V. Eschenroeder, B.E. Bode, J.E. Collier, D.C. Apperley, P.A. Cox, J.L. Casci, P.A. Wright, Micro. Meso. Mater 215 (2015) 154–167.
[27] U. Deka, I. Lezcano-Gonzalez, S.J. Warrender, A.L. Picone, P.A. Wright, B.M. Weckhuysen, A.M. Beale, Micro. Meso. Mater 166 (2013) 144–152.
[28] R. Martínez-Franco, M. Moliner, P. Concepcion, J.R. Thogersen, A. Corma, J. Catal 314 (2014) 73–82.
[29] R. Martinez-Franco, M. Moliner, C. Franch, A. Kustov, A. Corma, Appl. Catal. B Environ 127 (2012) 273–280.
[30] X. Xiang, M. Yang, B. Gao, Y. Qiao, P. Tian, S. Xu, Z. Liu, Rsc Adv 6 (2016) 12544–12552.
[31] Z. Liu, L. Yang, L. Xu, C. Sun, Y. Xiong, US Pat (2002) US6448197B1.
[32] W. Zhu, Y. Li, A. Xing, F. Li, S. Tian, CHN Pat. (2009) CN101555022B.
[33] J. Zhong, J. Han, Y. Wei, S. Xu, Y. He, Y. Zheng, M. Ye, X. Guo, C. Song, Z. Liu, Chem. Comm 54 (2018) 3146–3149.
[34] N.H.N. Kamarudin, A.A. Jalil, S. Triwahyono, R.R. Mukti, M.A.A. Aziz, H.D. Setiabudi, M.N.M. Muhid, H. Hamdan, Appl. Catal. A Gen 431-432 (2012) 104–112.
[35] X. Wang, W. Chen, L. Zhang, T. Yao, W. Liu, Y. Lin, H. Ju, J. Dong, L. Zheng, W. Yan, X. Zheng, Z. Li, X. Wang, J. Yang, D. He, Y. Wang, Z. Deng, Y. Wu, Y. Li, J. Am. Chem. Soc 139 (2017) 9419–9422.
[36] W. Shi, B. Zhang, Y. Lin, Q. Wang, Q. Zhang, D. Su, ACS Catal 6 (2016) 7844–7854.
[37] Y. Wang, J. Yao, H. Li, D. Su, M. Antonietti, J Am. Chem. Soc 133 (2011) 2362–2365.
[38] J. Xue, X. Wang, G. Qi, J. Wang, M. Shen, W. Li, J. Catal. 297(2013) 56–64.
[39] A.A. Gabrienko, S.S. Arzumanov, A.K. Toktarev, ACS Catal 7 (2017) 1818–1830.
[40] S. Tamiyakul, W. Ubolcharoen, D.N. Tungasmita, S. Jongpatiwut, Catal. Today 256 (2015) 325–335.
[41] Y. Jia, J. Wang, K. Zhang, S. Liu, G. Chen, Y. Yang, C. Ding, P. Liu, Catal. Sci. Tech 7 (2017) 1776–1791.
[42] R.A. Hunsicker, K. Klier, T.S. Gaffney, J.G. Kirner, Chem. Mater 14 (2002) 4807–4811.
[43] C. Song, X. Li, X. Zhu, S. Liu, F. Chen, F. Liu, L. Xu, Appl. Catal. A Gen 519 (2016) 48–55.
[44] P. Tian, B. Li, S. Xu, X. Su, D. Wang, L. Zhang, D. Fan, Y. Qi, Z. Liu, J Phy. Chem. C 117 (2013) 4048–4056.
[45] G. Liu, P. Tian, Y. Zhang, J. Li, L. Xu, S. Meng, Z. Liu, Micro. Meso. Mater 114 (2008) 416–423.
[46] C. Kong, J. Zhu, S.Y. Liu, Y. Wang, RSC Adv 7 (2017) 39889–39898.
[47] D.R. Dubois, D.L. Obrzut, J. Liu, J. Thundimadathil, P.M. Adekkanattu, J.A. Guin, A. Punnoose, M.S. Seehra, Fuel Pro. Tech 83 (2003) 203–218.
[48] M. Behrens, M. Armbrüster, Methanol steam reforming, in: L. Guczi, A. Erdôhelyi (Eds.), Catalysis for Alternative Energy Generation, Springer, New York, 2012, pp. 175–235.
[49] W.L. Dai, M. Scheibe, L. Li, N. Guan, M. Hunger, J. Phy. Chem. C 116 (2012) 2469–2476.
[50] W. Song, H. Fu, J.F. Haw, J Am. Chem. Soc 123 (2001) 4749–4754.
[51] W. Song, H. Fu, J.F. Haw, J Phy. Chem. B 105 (2001) 12839–12843.
[52] S. Muller, Y. Liu, F.M. Kirchberger, M. Tonigold, M. Sanchez-Sanchez, J.A. Lercher, J. Am. Chem. Soc 138 (2016) 15994–16003.